ChemComm

ROYAL SOCIETY OF CHEMISTRY

COMMUNICATION

View Article Online
View Journal

Check for updates

Cite this: DOI: 10.1039/d6cc01108j

Received 22nd February 2026,
Accepted 23rd April 2026

DOI: 10.1039/d6cc01108j

rsc.li/chemcomm

Fluoroalkyl-functionalized cyclic ethers as solvent for high-voltage batteries

Ke-Hsin Wang,[a] Ritesh Kumar,[a] Peiyuan Ma,[a] Jaemin Kim,[b]
Bitgaram Kim[a] and Chibueze V. Amanchukwu*[a]

A new class of side-chain-fluorinated cyclic ethers was studied for high voltage lithium metal batteries. Compared to linear fluorinated ethers, cyclic ethers maintain higher ionic conductivity despite increased ion pairing, while enhanced fluorination suppresses undesired solvent polymerization, improves oxidative stability, and enables long-term cycling with $LiNi_{0.8}Mn_{0.1}Co_{0.1}O_2$ (NMC811)-based cathodes.

The rise in electric vehicles has increased demand for high-energy-density batteries. Lithium metal anodes paired with nickel-rich high-voltage cathodes offer a promising solution due to the high theoretical capacity and large voltage difference. However, developing electrolytes compatible with both lithium anodes and high-voltage cathodes remains a challenge. Commercial carbonate-based electrolytes suffer from severe lithium dendrite growth and limited oxidative stability, restricting their performance.[1] In contrast, ethers have shown better compatibility with lithium metal, enabling more stable cycling but still suffer from poor oxidative stability.[2]

To further improve cathode compatibility, electrolyte engineering strategies include increasing salt concentration,[3] incorporating additives,[4,5] and optimizing cell design to build a stable interface.[6,7] Another approach is to modify the molecular structure of solvent molecules through fluorination, which lowers the HOMO (highest occupied molecular orbital) energy of solvent molecules and enhances oxidative stability.[8–10] Fluorination also weakens Li^+–solvent interactions, promoting cation–anion pairing and enriching the SEI (solid electrolyte interface) with beneficial inorganic components.[9–12] However, excessive fluorination decreases Li^+ affinity, hindering ion transport.[9] Yu *et al.* demonstrated that optimizing the degree of fluorination is key to balancing these effects.[13] Their work identified F5DEE (2-[2-(2,2-difluoroethoxy)-ethoxy]-1,1,1-trifluoroethane) as a solvent that achieves both oxidative stability and sufficient ionic conductivity, enabling stable cycling in full cells with high-voltage cathodes.

However, there have been limited studies on fluorinated cyclic ethers. In our prior work, we synthesized and studied mono-fluorinated cyclic ethers such as 3FTHF (3-fluorotetrahydrofuran).[14] We showed that with fluorination on the 3′ position, 3FTHF demonstrates high lithium compatibility and high ionic conductivity, but the solvent polymerization at 4.4 V in 1 M LiFSA (lithium bis(fluorosulfonyl)amide) electrolyte limited its use with $LiNi_{0.8}Mn_{0.1}Co_{0.1}O_2$ (NMC811) cathodes. Here, we increase the fluorination content of the cyclic ethers to suppress polymerization and enable higher voltage cathodes. We systematically explore heavily fluorinated cyclic ethers and use asymmetric side-chain fluorination to preserve the oxygen coordination site on the ring, maintaining salt solubility. The impacts of degree of fluorination on the physicochemical properties, lithium-ion solvation, oxidative stability, and lithium compatibility were studied. With fluoroalkyl chain on the 3′ position of THF (Fig. 1), we preserve the lithium compatibility of 3FTHF and improve the oxidative stability of the electrolyte containing 1 M LiFSA in these cyclic ethers.

Four fluoroalkyl cyclic ethers shown in Fig. 1 are synthesized and characterized (Fig. S1 and S2). Cyclic ethers with fluoroalkyl chains on the 2′ position show chemical instability with addition of LiFSA and are therefore not discussed in detail in this study (Fig. S3). We investigated the effect of fluorination on ionic conductivity and Fig. 2a shows that increased fluorine content lowers the room temperature ionic conductivity (Table S1).

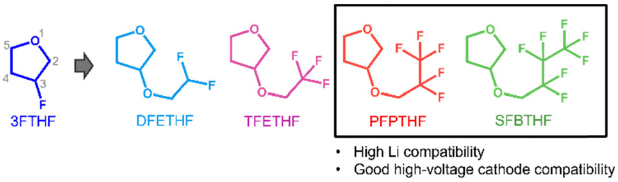

Fig. 1 Molecular structure design based on increasing the fluorination degree of 3-fluorotetrahydrofuran (3FTHF): DFETHF, TFETHF, PFPTHF, and SFBTHF. Full names in SI. Grey values by the atoms on 3FTHF indicate the atom-position numbering.

---

[a] *Pritzker School of Molecular Engineering, University of Chicago, IL 60637, USA. E-mail: chibueze@uchicago.edu*

[b] *Department of Chemistry, University of Chicago, Chicago, IL 60637, USA*

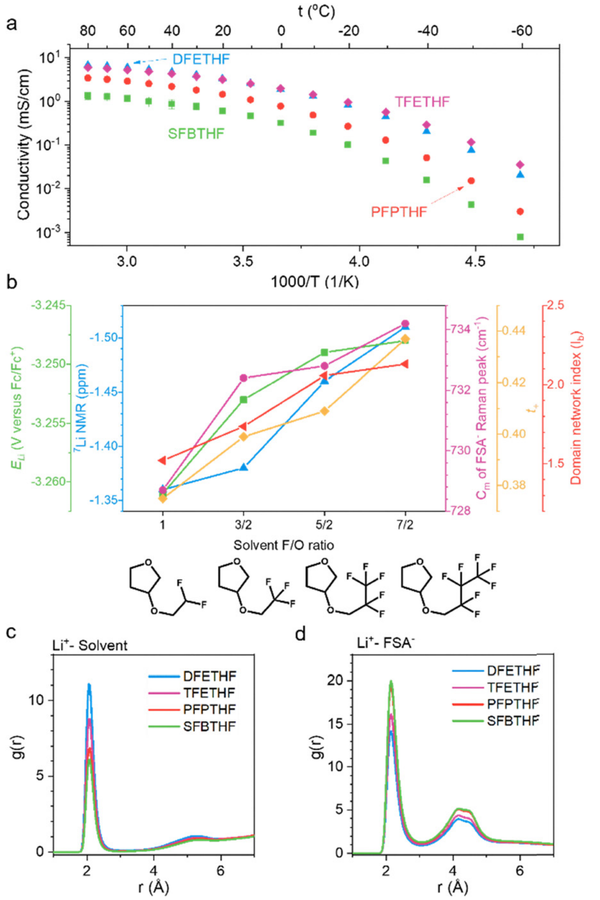

Fig. 2 Physicochemical properties. (a) Temperature-dependent ionic conductivity of electrolytes containing 1 M LiFSA in fluoroalkyl cyclic ethers. (b) Trend of solvation related properties upon increasing fluorination degree. Methods tested in this work include Li potential[17] (E_{Li}), peak position of ^{7}Li NMR, center of mass (C_m) of FSA$^-$ Raman peak, lithium transference number (t_+), and calculated domain network index (I_b).[18] (c and d) Classical molecular dynamics (CMD) simulations of fluorinated cyclic ethers with different fluorination degrees using ByteFF-Pol force field. (c) Radial distribution function (RDF) between Li$^+$ and solvent molecules. (d) RDF between Li$^+$ and FSA$^-$.

However, TFETHF is an exception, exhibiting conductivity comparable to DFETHF at room temperature and even surpassing it at low temperatures (<0 °C). This behavior is likely due to the lower viscosity of TFETHF compared to its partially fluorinated counterpart, DFETHF.[13] The perfluoro groups (–CF$_3$) in TFETHF present weaker intermolecular forces with other polar species, including solvent molecules and ions, than the partially-fluorinated counterparts (–CHF$_2$).[15] As a result, TFETHF shows lower viscosity than DFETHF in both pure solvents and electrolytes (Table S1) and higher diffusivity ($D_{Li^+} = 0.63 \times 10^{-10}$ m^2 s^{-1} for DFETHF and $D_{Li^+} = 0.80 \times 10^{-10}$ m^2 s^{-1} for TFETHF). To further analyze the impact of fluorination, we define the F/O ratio as the number of fluorine atoms relative to oxygen atoms in the solvent molecule. Despite having an F/O ratio of 3.5, higher than all the linear fluorinated ethers reported by Yu *et al.*, SFBTHF can still dissolve 1 M LiFSA and exhibits an ionic conductivity slightly exceeding the conductivity of 1.2 M LiFSA in F6DEE (F/O = 3, 0.053 mS cm^{-1} for SFBTHF *versus* 0.045 mS cm^{-1} for F6DEE).[16] This finding allows us to explore a molecular family with high fluorine content while maintaining moderate conductivity.

The solvation structure of an electrolyte plays a crucial role in determining its compatibility with both anodes and cathodes. When Li$^+$ is weakly solvated by the solvent, FSA$^-$ more readily contributes to the formation of solid–electrolyte[19–21] (SEI) and cathode–electrolyte[19,22,23] (CEI) interfaces, leading to inorganic-rich layers that have been reported to enhance interfacial stability and reduce capacity loss during cycling.

To assess solvation structure trends across the four studied electrolytes, we employed four experimental characterization techniques and classical molecular dynamics (CMD) using polarizable ByteFF-Pol force field[24] (comparison to the widely used non-polarizable optimized potentials for liquid simulations (OPLS) force field[25] in Fig. S4), as shown in Fig. 2b. The electrolytes are arranged from left to right based on the F/O ratio of the solvent molecular structure. First, we measured the lithium potential (E_{Li}) *via* cyclic voltammetry using 1 mM ferrocene (Fc) as a reference following the method developed by Ko *et al.*[17] Electrolytes with less negative E_{Li} represent those with stronger Li$^+$–FSA$^-$ interactions and have been found to more effectively prevent reductive electrolyte degradation. Among the electrolytes, SFBTHF shows the least negative E_{Li}, representing the strongest Li$^+$–FSA$^-$ pairing. Second, ^{7}Li NMR spectra reveal that the Li$^+$ peak in SFBTHF shifts upfield, suggesting increased electron density donation from FSA$^-$ to Li$^+$. Third, Raman spectroscopy of the S–N–S stretching mode in FSA$^-$ (720–750 cm^{-1}) allows deconvolution of solvation structures,[26,27] showing that higher fluorination shifts the dominant Li$^+$ solvation from solvent-separated ion pairs (SSIPs) in DFETHF and TFETHF to contact ion pairs (CIPs) in PFPTHF and SFBTHF (Fig. S5). Solvation energy of CIP solvation cluster (extracted from CMD trajectory) for the four electrolytes calculated using density functional theory (DFT) also confirms this trend (Fig. S6). The CIP solvation energy values are strongest in SFBTHF (−1.88 eV), followed by PFPTHF (−1.80 eV), TFETHF (−1.77 eV), and DFETHF (−1.74 eV), implying that the ion pair formation is thermodynamically most favorable in SFBTHF compared to other electrolytes. This trend confirms that heavy fluorination promotes stronger Li$^+$–FSA$^-$ associations. At a broader scale, enhanced cation–anion interaction increases the size of Li$^+$–FSA$^-$ networks, quantified by the domain network index[18] (red trace in Fig. 2b), ultimately leading to decrease in ionic conductivity at room temperature.

Additionally, Li$^+$–FSA$^-$ interactions influence the conductivity (Note S1 and Fig. S7) and Li$^+$ transference number (t_+), calculated as $t_+ = D_{Li^+}/(D_{Li^+} + D_{FSA^-})$, where D_{Li^+} and D_{FSA^-} refers to the diffusivity of the cation and anion respectively measured with pulsed field gradient nuclear magnetic resonance (PFG-NMR) (Table S2) spectroscopy. Typically, Li$^+$ interacts more strongly with solvents than bulkier anions, leading to slower Li$^+$ transport. However, when Li$^+$–FSA$^-$ interactions are strong, FSA$^-$ assists in Li$^+$ motion, increasing t_+.[28] We observe that more heavily fluorinated solvents exhibit higher t_+, consistent with stronger Li$^+$–FSA$^-$ interactions in these electrolytes. Fig. 2b summarizes the five solvation characterization methods described above, showing a transition from solvent-dominated Li^+ solvation to strong Li^+–FSA^- pairing as the F/O ratio increases.

Several factors may contribute to the observed correlation between higher F/O ratio and stronger Li^+–FSA^- interactions observed in this study. First, fluorine atoms act as electron-withdrawing groups, reducing the electron density at the primary Li^+ coordination site of the solvent molecules. For the fluorinated cyclic ethers investigated here, the oxygen atom in the THF ring serves as the dominant coordination site (Fig. S8), potentially due to more negative electrostatic potential compared to the oxygen atom outside the ring (Fig. S9). In addition to electronic effects, steric hindrance from bulky fluorinated substituents may further weaken Li^+–solvent coordination. Radial distribution functions (RDFs) of Li^+–solvent interactions capture the combined influence of decreased electron density and increased steric hindrance, showing progressively weaker Li^+–solvent coordination from DFETHF to SFBTHF (Fig. 2c). As Li^+–solvent interactions weaken, more anions can enter the first solvation shell, resulting in a higher degree of ion pairing (Fig. 2d), consistent with observations from Raman spectroscopy.

In a previous study, we developed a monofluorinated cyclic ether, 3FTHF[14] (F/O = 1), which exhibits fast ion transport and is well suited for low-temperature lithium battery applications. Table S3 shows that 3FTHF and DFETHF, which share the same F/O ratio, exhibit similar degrees of ion pairing. However, due to the higher molecular weight of DFETHF, its ionic conductivity is more than twofold lower, making 3FTHF the more favorable choice for low-temperature operation. Notably, similar F/O ratios do not necessarily imply identical Li^+ solvation structures. Compared to previously reported fluorinated linear ethers[13] with the same F/O ratio, cyclic ether electrolytes fluorinated at the 3′ position of THF show stronger Li^+–solvent solvation. Explanation and discussion for this structural effect are in Note S2 and Fig. S9 and S10.

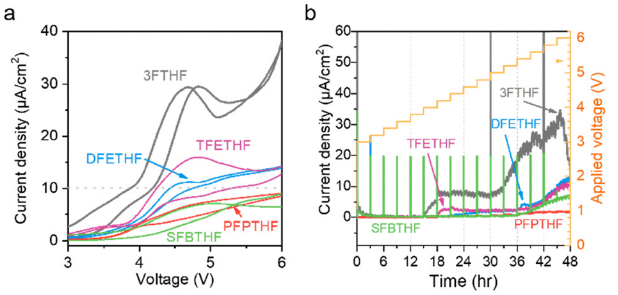

Fig. 3 Oxidative stability. (a) Linear sweep voltammetry (LSV) of Li||Al coin cells using electrolytes containing 1 M LiFSA in fluoroalkyl cyclic ethers. The voltage is swept from open circuit to 6 V at 1 mV s^{-1}. A dashed line of leakage current at 0.01 mA cm^{-2} is drawn for easier comparison. Two cells of each electrolyte are shown with the same color. (b) Potentiostatic hold results of 1 M LiFSA in fluoroalkyl cyclic ethers in comparison with a monofluorinated ether, 3FTHF. The voltage is swept from 3.0 V to 6.0 V with a 0.2 V step. The data of 3FTHF is adapted from our prior work.[14] Voltages are *vs.* Li/Li^+.

Previous studies, including our own,[14] have shown that nonfluorinated[29] and mono-fluorinated cyclic ethers tend to polymerize at high voltages, limiting their compatibility with high-voltage cathodes. The issue is addressed in heavily fluorinated ethers presented in this work, where we demonstrate an improvement in oxidative stability (Fig. 3 and Fig. S11) and the absence of polymer found in cycled electrolytes (Fig. S12). As shown in Fig. 3a, the strong leakage current presented in 3FTHF at around 4.4 V is suppressed by half in DFETHF and TFETHF. Further increasing the fluorination degree (F/O $\geq$ 2.5) leads to well-suppressed leakage current ($<$0.01 mA cm^{-2}) up to 6.0 V. The improved oxidative stability is further demonstrated by subjecting the cells to a voltage step from 3.0 V to 6.0 V (Fig. 3b), where PFPTHF and SFBTHF maintains a leakage current below 10 μA cm^{-2} throughout the test, whereas 3FTHF shows a sharp increase in leakage current at 4.0 V, reaching 30 μA cm^{-2} near 6.0 V. In addition, we observe that increasing the degree of fluorination effectively enhances oxidative stability by suppressing voltage-induced polymerization up to 4.4 V, the typical upper cutoff for NMC811 cathodes. No new peaks were observed in NMR (Fig. S12) after holding the cell using TFETHF-based electrolytes at 4.4 V, unlike the polymerization reaction that happens in the cell using 3FTHF-based electrolytes.[14]

The enhanced oxidative stability observed when more fluorine atoms are directly incorporated into the solvent molecular structure can be partially attributed to the lowering of the highest occupied molecular orbital (HOMO) level (Fig. S13), as calculated by DFT. The results on full cell cycling will be discussed later.

We previously reported[14] that the position of mono-fluorination significantly influences lithium compatibility. Herein, we found that electrolytes functionalized at the 3’ position with a fluoroalkyl side chain exhibit high lithium compatibility, with Li||Cu Coulombic efficiencies (CE) exceeding 97% (Fig. 4a) and granular lithium deposition observed under scanning electron microscopy (SEM) (Fig. S14). Among these electrolytes, PFPTHF (99.53%) and SFBTHF (98.44%) achieve higher CE than DFETHF (97.61%) and TFETHF (97.00%). Their slightly higher cycling overpotentials are reflected in the critical current density test shown in Fig. 4b. When the applied current density increase to 2 mA cm^{-2}, Li||Li cells using PFPTHF and SFBTHF show unstable voltage as a sign of soft shorting[31] which is likely due to insufficient ionic conductivity. The limited performance at high current density may explain the early failure of Li||Li symmetric cells cycled at 1 mA cm^{-2} with SFBTHF as the electrolyte, which can be addressed by introducing a diluent to the electrolyte (Fig. S15).

Despite their limitations at high current density (Fig. S16a), PFPTHF and SFBTHF electrolytes show both superior full cell cycling in thin Li||LFP configuration (Fig. S16b) and high compatibility with widely used nickel-rich, high-voltage cathodes (NMC811, $LiNi_{0.8}Mn_{0.1}Co_{0.1}O_2$, 3.0 to 4.4 V), as demonstrated in Fig. 4d and Fig. S16c. Specifically, Li||NMC811 cells using SFBTHF electrolyte achieve 80% capacity retention after 197 cycles (averaged over two cells), overcoming the disadvantage of 3FTHF studied previously and proving the capability of fluorinated cyclic ethers in high-voltage applications (discussion of cathode failure in Note S3 and Fig. S17). With similar initial CE values (81%, Fig. S18), the observed cycle life trend among the four fluoroalkyl cyclic ethers proposed in this work

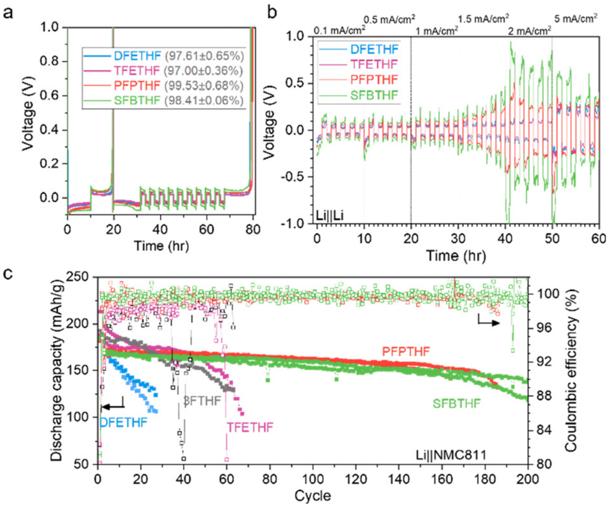

Fig. 4 Battery cycling performance. (a) Coulombic efficiency (CE) of Li||Cu coin cells using electrolytes containing 1 M LiFSA in fluoroalkyl cyclic ethers by Aurbach method.[30] (b) Critical current density test of 1 M LiFSA in fluoroalkyl cyclic ethers in Li||Li symmetric cells. The cells were cycled with charge/discharge time fixed at 1 h and current densities indicated in the text above the figure. (c) Galvanostatic cycling of Li||NMC811 half cell at *C*/3 (≈0.55 mA cm^{-2}). NMC811 loading ≈1.66 mA h cm^{-2}. Replicates of each electrolyte are shown. NMC811: $LiNi_{0.8}Mn_{0.1}Co_{0.1}O_2$. Voltages are *vs.* Li/Li$^+$.

aligns well with the oxidative stability results from Li||Al cells (Fig. 3a) and correlates with the degree of fluorination (DFETHF < TFETHF < PFPTHF and SFBTHF). While CEI analysis by X-ray photoelectron spectroscopy (XPS) (Fig. S19) does not reveal significant compositional differences, the strong correlation between the oxidative stability in Fig. 3 and Li||NMC811 cycle life indicates that heavy fluorination is an effective strategy for improving cathode stability. Additionally, XPS analysis of lithium metal reveals a more inorganic-rich surface containing richer Li_2O and LiF for heavily fluorinated electrolytes, indicating a potential SEI-stabilizing effect with increasing fluorination degree (Fig. S20 and S21 and Note S4).

In this work, we demonstrated that increasing solvent fluorination through side-chain modification enhances both lithium compatibility and high-voltage cathode stability in cyclic fluorinated ethers. A key advantage of 3′ position fluorination is that it maintains sufficient ionic conductivity even at high fluorination degrees. As a result, electrolytes based on heavily fluorinated PFPTHF and SFBTHF exhibit improved cycling performance in both 20 μm Li||LFP full cells and Li||NMC811 cells.

Conflicts of interest

There are no conflicts of interest to declare.

Data availability

The data supporting this article have been included as part of the supplementary information (SI). Supplementary information: including synthetic scheme (Fig. S1), NMR spectra (Fig. S2, S3, and S12), MD calculation data (Fig. S4 and S8, Table S4), conductivity data (Table S1), solvation properties data (Fig. S5, S7, S10, Table S2 and S3), DFT data (Fig. S6, S9, and S113), leakage current data (Fig. S11), SEM images (Fig. S14), battery cycling data (Fig. S15, S16, and S18), XPS spectra (Fig. S19 and S20), and titration data (Fig. S21). See DOI: https://doi.org/10.1039/d6cc01108j.

Acknowledgements

This work was primarily supported by the National Science Foundation (NSF) CAREER Award (CBET-2144454). NMR was performed at the University of Chicago Department of Chemistry NMR facility. SEM and Raman spectroscopy were conducted at the University of Chicago Materials Research Science and Engineering Center (MRSEC). XPS was performed at the Northwestern University's Atomic and Nanoscale Characterization Experimental Center (NUANCE). The DFT calculations and MD simulations were conducted with resources provided by the University of Chicago's Research Computing Center. The authors acknowledge support from Steve Trask and Andrew Jansen at Argonne's Cell Analysis, Modeling, and Prototyping (CAMP) facility for providing the LFP and NMC811 cathode. R. K. acknowledges support from the Eric and Wendy Schmidt AI in Science Fellowship at the University of Chicago, a Schmidt Sciences program.

References

1 Z. Li, Y. Chen, X. Yun, P. Gao, C. Zheng and P. Xiao, Critical Review of Fluorinated Electrolytes for High-Performance Lithium Metal Batteries, *Adv. Funct. Mater.*, 2023, **33**(32), 2300502, DOI: 10.1002/adfm.202300502.
2 D. Lin, Y. Liu and Y. Cui, Reviving the Lithium Metal Anode for High-Energy Batteries, *Nat. Nanotechnol.*, 2017, **12**(3), 194–206, DOI: 10.1038/nnano.2017.16.
3 X. Ren, L. Zou, S. Jiao, D. Mei, M. H. Engelhard, Q. Li, H. Lee, C. Niu, B. D. Adams, C. Wang, J. Liu, J.-G. Zhang and W. Xu, High-Concentration Ether Electrolytes for Stable High-Voltage Lithium Metal Batteries, *ACS Energy Lett.*, 2019, **4**(4), 896–902, DOI: 10.1021/acsenergylett.9b00381.
4 W. Zhang, Y. Lu, L. Wan, P. Zhou, Y. Xia, S. Yan, X. Chen, H. Zhou, H. Dong and K. Liu, Engineering a Passivating Electric Double Layer for High Performance Lithium Metal Batteries, *Nat. Commun.*, 2022, **13**(1), 2029, DOI: 10.1038/s41467-022-29761-z.
5 H. Wang, J. Zhang, H. Zhang, W. Li, M. Chen, Q. Guo, K. C. Lau, L. Zeng, G. Feng, D. Zhai and F. Kang, Regulating Interfacial Structure Enables High-Voltage Dilute Ether Electrolytes, *Cell Rep. Phys. Sci.*, 2022, **3**(6), 100919, DOI: 10.1016/j.xcrp.2022.100919.
6 Q. An, Q. Liu, P. Mao, L. Duan, H. Y. Zhu, L. Liu, G. Zhao, Y. Zha, L. Yang, M. Sun, Y. Fan, F. Xie, G. Hu and H. Guo, Developing the Tandem Structure to Regulate Interfacial Chemistry and Promote Ion Transport Kinetics toward High-Voltage Lithium Metal Batteries, *Angew. Chem., Int. Ed.*, 2025, **64**(19), e202422539, DOI: 10.1002/anie.202422539.
7 Y. Tian, Z. Pei, D. Luan and X. W. Lou, In Situ Anchoring 2d Hexagonal Zn-Mof on Mxene toward Robust Anode-Less 5 V–Class Li Metal Batteries, *Sci. Adv.*, 2026, **12**(5), eaeb1378, DOI: 10.1126/sciadv.aeb1378(acccessed 2026/03/14).
8 T. Zhou, Y. Zhao, M. El Kazzi, J. W. Choi and A. Coskun, Integrated Ring-Chain Design of a New Fluorinated Ether Solvent for High-Voltage Lithium-Metal Batteries, *Angew. Chem., Int. Ed.*, 2022, **61**(19), e202115884, DOI: 10.1002/anie.202115884.
9 L. Q. Wu, Z. Li, Z. Y. Fan, K. Li, J. Li, D. Huang, A. Li, Y. Yang, W. Xie and Q. Zhao, Unveiling the Role of Fluorination in Hexacyclic Coordinated

Ether Electrolytes for High-Voltage Lithium Metal Batteries, *J. Am. Chem. Soc.*, 2024, **146**(9), 5964–5976, DOI: 10.1021/jacs.3c11798.

10 Y. Zhao, T. Zhou, M. Mensi, J. W. Choi and A. Coskun, Electrolyte Engineering Via Ether Solvent Fluorination for Developing Stable Non-Aqueous Lithium Metal Batteries, *Nat. Commun.*, 2023, **14**(1), 299, DOI: 10.1038/s41467-023-35934-1.

11 I. R. Choi, Y. Chen, A. Shah, J. Florian, C. Serrao, J. Holoubek, H. Lyu, E. Zhang, J. H. Lee, Y. Lin, S. C. Kim, H. Park, P. Zhang, J. Lee, J. Qin, Y. Cui and Z. Bao, Asymmetric Ether Solvents for High-Rate Lithium Metal Batteries, *Nat. Energy*, 2025, **10**, 365–379, DOI: 10.1038/s41560-025-01716-w.

12 Y. Zhao, T. Zhou, M. El Kazzi and A. Coskun, Fluorinated Cyclic Ether Co-Solvents for Ultra-High-Voltage Practical Lithium-Metal Batteries, *ACS Appl. Energy Mater.*, 2022, **5**(6), 7784–7790, DOI: 10.1021/acsaem.2c01261.

13 Z. Yu, P. E. Rudnicki, Z. Zhang, Z. Huang, H. Celik, S. T. Oyakhire, Y. Chen, X. Kong, S. C. Kim, X. Xiao, H. Wang, Y. Zheng, G. A. Kamat, M. S. Kim, S. F. Bent, J. Qin, Y. Cui and Z. Bao, Rational Solvent Molecule Tuning for High-Performance Lithium Metal Battery Electrolytes, *Nat. Energy*, 2022, **7**(1), 94–106, DOI: 10.1038/s41560-021-00962-y.

14 K. H. Wang, P. Ma, J. Kim, M. Han and C. V. Amanchukwu, Monofluorinated Cyclic Ethers Enable Fast Ion Transport in Low-Temperature Lithium Metal Batteries, *ACS Appl. Mater. Interfaces*, 2025, **17**(24), 35606–35618, DOI: 10.1021/acsami.5c07377.

15 C. Dalvit, C. Invernizzi and A. Vulpetti, Fluorine as a Hydrogen-Bond Acceptor: Experimental Evidence and Computational Calculations, *Chemistry*, 2014, **20**(35), 11058–11068, DOI: 10.1002/chem.201402858.

16 Z. Yu, H. Wang, X. Kong, W. Huang, Y. Tsao, D. G. Mackanic, K. Wang, X. Wang, W. Huang, S. Choudhury, Y. Zheng, C. V. Amanchukwu, S. T. Hung, Y. Ma, E. G. Lomeli, J. Qin, Y. Cui and Z. Bao, Molecular Design for Electrolyte Solvents Enabling Energy-Dense and Long-Cycling Lithium Metal Batteries, *Nat. Energy*, 2020, **5**(7), 526–533, DOI: 10.1038/s41560-020-0634-5.

17 S. Ko, T. Obukata, T. Shimada, N. Takenaka, M. Nakayama, A. Yamada and Y. Yamada, Electrode Potential Influences the Reversibility of Lithium-Metal Anodes, *Nat. Energy*, 2022, **7**(12), 1217–1224, DOI: 10.1038/s41560-022-01144-0.

18 R. Li, H. Zhang, S. Zhang, Y. Li, R. Guo, H. Pei, M. Yang, J. Zhang, L. Chen, X. Xiao, L. Chen, Y. Shen, T. Deng and X. Fan, Unified Affinity Paradigm for the Rational Design of High-Efficiency Lithium Metal Electrolytes, *Nat. Energy*, 2025, **10**, 1155–1165, DOI: 10.1038/s41560-025-01842-5.

19 K. Ding, C. Xu, Z. Peng, X. Long, J. Shi, Z. Li, Y. Zhang, J. Lai, L. Chen, Y. P. Cai and Q. Zheng, Tuning the Solvent Alkyl Chain to Tailor Electrolyte Solvation for Stable Li-Metal Batteries, *ACS Appl. Mater. Interfaces*, 2022, **14**(39), 44470–44478, DOI: 10.1021/acsami.2c13517.

20 A. M. Li, O. Borodin, T. P. Pollard, W. Zhang, N. Zhang, S. Tan, F. Chen, C. Jayawardana, B. L. Lucht, E. Hu, X. Q. Yang and C. Wang, Methylation Enables the Use of Fluorine-Free Ether Electrolytes in High-Voltage Lithium Metal Batteries, *Nat. Chem.*, 2024, **16**, 922–929, DOI: 10.1038/s41557-024-01497-x.

21 Y. Xue, Y. Wang, H. Zhang, W. Kong, Y. Zhou, B. Kang, Z. Huang and H. Xiang, Molecular Design of Mono-Fluorinated Ether-Based Electrolyte for All-Climate Lithium-Ion Batteries and Lithium-Metal Batteries, *Angew. Chem., Int. Ed.*, 2024, e202414201, DOI: 10.1002/anie.202414201.

22 Z. Piao, X. Wu, H. R. Ren, G. Lu, R. Gao, G. Zhou and H. M. Cheng, A Semisolvated Sole-Solvent Electrolyte for High-Voltage Lithium Metal Batteries, *J. Am. Chem. Soc.*, 2023, **145**(44), 24260–24271, DOI: 10.1021/jacs.3c08733.

23 Z. Li, H. Rao, R. Atwi, B. M. Sivakumar, B. Gwalani, S. Gray, K. S. Han, T. A. Everett, T. A. Ajantiwalay, V. Murugesan, N. N. Rajput and V. G. Pol, Non-Polar Ether-Based Electrolyte Solutions for Stable High-Voltage Non-Aqueous Lithium Metal Batteries, *Nat. Commun.*, 2023, **14**(1), 868, DOI: 10.1038/s41467-023-36647-1.

24 T. Zheng; X. Xu; Z. Wang; Z. Yang; Y. Wang; X. Han; L. Chen; Z. Mu; Z. Zhang; S. Liu; S. Gong; K. Yu and W. Yan, Bridging Quantum Mechanics to Organic Liquid Properties Via a Universal Force Field, *arXiv*, 2025, preprint, arXiv:2508.08575, DOI: 10.48550/arXiv.2508.08575.

25 G. A. Kaminski, R. A. Friesner, J. Tirado-Rives and W. L. Jorgensen, Evaluation and Reparametrization of the Opls-Aa Force Field for Proteins Via Comparison with Accurate Quantum Chemical Calculations on Peptides, *J. Phys. Chem. B*, 2001, **105**(28), 6474–6487, DOI: 10.1021/jp003919d.

26 S.-D. Han, O. Borodin, D. M. Seo, Z.-B. Zhou and W. A. Henderson, Electrolyte Solvation and Ionic Association, *J. Electrochem. Soc.*, 2014, **161**(14), A2042–A2053, DOI: 10.1149/2.0101414jes.

27 S.-D. Han, R. D. Sommer, P. D. Boyle, Z.-B. Zhou, V. G. Young, O. Borodin and W. A. Henderson, Electrolyte Solvation and Ionic Association: Part Ix. Structures and Raman Spectroscopic Characterization of Lifsi Solvates, *J. Electrochem. Soc.*, 2022, **169**(11), 110544, DOI: 10.1149/1945-7111/ac9a07.

28 J. Zhao, L. Wang, X. He, C. Wan and C. Jiang, Determination of Lithium-Ion Transference Numbers in Lipf6–Pc Solutions Based on Electrochemical Polarization and Nmr Measurements, *J. Electrochem. Soc.*, 2008, **155**(4), A292–A296, DOI: 10.1149/1.2837832.

29 A. N. Dey and E. J. Rudd, Electroinitiated Polymerization of Tetrahydrofuran, *J. Electrochem. Soc.*, 1974, **121**, 1294–1299, DOI: 10.1149/1.2401671.

30 B. D. Adams, J. Zheng, X. Ren, W. Xu and J. G. Zhang, Accurate Determination of Coulombic Efficiency for Lithium Metal Anodes and Lithium Metal Batteries, *Adv. Energy Mater.*, 2017, **8**(7), 1702097, DOI: 10.1002/aenm.201702097.

31 S. Menkin, J. B. Fritzke, R. Larner, C. de Leeuw, Y. Choi, A. B. Gunnarsdottir and C. P. Grey, Insights into Soft Short Circuit-Based Degradation of Lithium Metal Batteries, *Faraday Discuss.*, 2024, **248**(0), 277–297, DOI: 10.1039/d3fd00101f.